# Projective measurements in quantum and classical optical systems

Filippus S. Roux* and Yingwen Zhang
*CSIR National Laser Centre, P.O. Box 395, Pretoria 0001, South Africa*
(Received 3 July 2014; published 22 September 2014)

Experimental setups for the optical implementation of projective measurements in the Laguerre-Gaussian basis are discussed. Special attention is given to the case where the measurements are made with the aid of single-mode fibers that are used to extract the Gaussian component from an optical distribution. Although this setup can, under some conditions, implement the inner product operation accurately, the overlap with the Gaussian mode in the single-mode fiber often produces cross-talk among Laguerre-Gaussian modes with different radial indices. The extent of the cross-talk is analyzed quantitatively.

DOI: 10.1103/PhysRevA.90.033835 PACS number(s): 42.50.Dv, 03.65.Wj, 42.50.Tx, 42.50.Ex

## I. INTRODUCTION

In many quantum, and also classical, optical applications the need exists to perform projective measurements. One particular application is quantum state tomography [1], which is used to determine the density matrix of a photonic quantum state. Although, the front ends and back ends (sources and detectors) of classical and quantum optical systems are in general different, the optical system between the front end and back end of a quantum optical system that performs projective measurements on photons will perform the same task on a classical optical beam. For this reason, the discussion here applies equally well to both classical and quantum optical systems.

A projective measurement, in the context of quantum mechanics, is understood to be the process where a projection operator operates on some input state. Often this projection operator is composed of a single basis element, and can as such be represented by $\mathcal{P} = |\Phi_n\rangle\langle\Phi_n|$. The result of this projection on an input state $|\psi\rangle$ is given by $\mathcal{P}|\psi\rangle = |\Phi_n\rangle\langle\Phi_n|\psi\rangle$. When the input state is a photon state, the measurement destroys the photon so that one can express the projection simply in terms of the inner product $\langle\Phi_n|\psi\rangle$. The measured quantity would be proportional to $|\langle\Phi_n|\psi\rangle|^2$. In other words, to implement a projective measurement in an optical system, one needs to implement an inner product.

There have been various classical implementations of inner products in optical systems. The VanderLugt optical correlator [2] can be seen as an optical implementation of an inner product. One can also use diffractive optical elements to implement so-called diffractive optical inner-product transforms, which have been used to extract features for optical pattern recognition applications [3]. This technology has recently been reinvented to do modal decompositions of the electric fields inside novel multimode optical fibers [4].

In quantum information systems, projective measurements are routinely done to perform quantum state tomography [1] or to measure the modal spectra of output quantum states [5]. However, as was pointed out recently [6], such measurements can lead to errors in the measured values of the coefficients. The reason for these errors is related to the fact that in these experiments a single-mode fiber (SMF) is used to extract the Gaussian modal content from the field incident on the fiber end. The overlap integral that gives the coupling constant for the light coupling into the fiber does not resemble the required inner product integral. The difference between the overlap integral and the inner product integral gives rise to an inaccurate estimate of the projective measurement. The situation is in fact even more severe: due to the distortion of the inner product integral, different modes are not in general orthogonal with respect to this distorted inner product. As a result, there is cross-talk among the different modes.

In this paper, we investigate different experimental setups that can accurately perform optical projective measurements (inner products). First, we described the different optical setups that can be used to perform inner products and we provide their mathematical models. The conditions under which these setups would perform accurate projective measurements are discussed. One of these setups, which incorporates an SMF, is analyzed in more detail to demonstrate the cross-talk that can occur due to the distortion caused by the Gaussian overlap.

The discussion is done in the context of the Laguerre-Gaussian (LG) basis, which is widely used because the LG modes are orbital angular momentum (OAM) eigenmodes [7]. However, the conclusions of this investigation also applies to other sets of orthogonal functions, such as the Bessel-Gaussian modes [8].

## II. EXPERIMENTAL SETUPS

The expression for the inner product that is used in the optical application under consideration is given by

$$\langle f,g\rangle = \iint_{\mathcal{D}} f(\mathbf{x})g^*(\mathbf{x})\,d^2x, \tag{1}$$

where $\mathcal{D}$ is the domain of integration, namely, the entire transverse plane, $f(\mathbf{x})$ and $g(\mathbf{x})$ are two-dimensional normalized complex-valued functions,[1] the two-dimensional transverse position vector is denoted by $\mathbf{x}$, and $*$ denotes the complex conjugate. The normalization of $f(\mathbf{x})$ is defined by

$$\iint_{\mathcal{D}} |f(\mathbf{x})|^2\,d^2x = 1, \tag{2}$$

*fsroux@csir.co.za

[1] In the context of quantum mechanics, $f(\mathbf{x})$ can be interpreted as the two-dimensional wave function of the quantum state: $f(\mathbf{x}) = \langle\mathbf{x}|f\rangle$ and the same for $g(\mathbf{x})$.

 

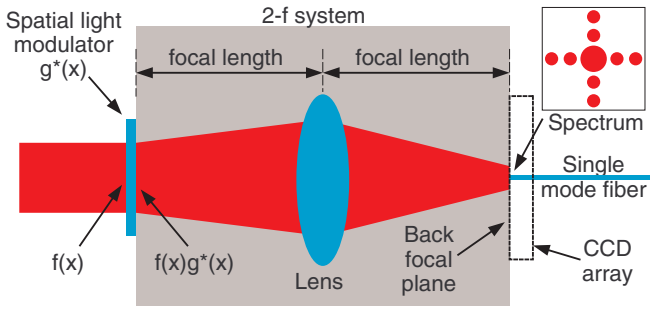


FIG. 1. (Color online) Diagram of a system that performs projective measurements by coupling (the central part of) the Fourier transform of $f(\mathbf{x})g^*(\mathbf{x})$ into an SMF. For classical applications, the light can be measured by a CCD pixel at the origin.

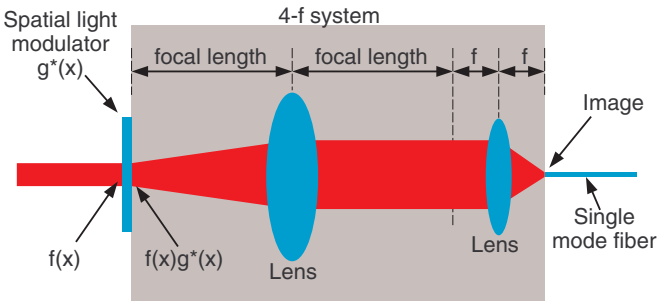


FIG. 2. (Color online) Diagram of a system that performs projective measurements by imaging the product $f(\mathbf{x})g^*(\mathbf{x})$ onto the end of an SMF.

and the same for $g(\mathbf{x})$. Henceforth, we drop the $\mathcal{D}$. In an optical system, $f(\mathbf{x})$ would represent the complex distribution of the optical field. To perform the inner product, $f(\mathbf{x})$ first needs to be multiplied by $g^*(\mathbf{x})$. This is done by modulating the optical field with a complex-valued transmission function, which can be implemented with the aid of a diffractive optical element or a spatial light modulator (SLM). For the sake of the subsequent discussion we'll assume that an SLM is used for this purpose. The result behind the SLM then needs to be integrated to complete the process for the inner product.

The physical transmission (or reflection) function of the SLM is not normalized and therefore is only proportional to the normalized function $g^*(\mathbf{x})$ encoded on it. The proportionality constant is obtained from the loss in optical power when a plane wave is modulated by that SLM. In the discussions below, we will ignore this constant.

### A. Fourier approach

There are different approaches to implementing the final integration optically. The first approach employs an optical Fourier transform, as shown in Fig. 1. Passing the modulated optical field $f(\mathbf{x})g^*(\mathbf{x})$ through a 2-f system, one obtains the Fourier transform of the product of the two functions. This gives

$$\begin{aligned}\mathcal{F}\{fg^*\} &= \iint f(\mathbf{x})g^*(\mathbf{x})\exp[i2\pi(ax+by)]\,d^2x \\ &= \tilde{f}(\mathbf{a})\otimes\tilde{g}(\mathbf{a}),\end{aligned} \tag{3}$$

where $\mathcal{F}\{\cdot\}$ represents the Fourier transform operation and $\otimes$ denotes the correlation operation. The output is the cross-correlation of the spectra $\tilde{f}(\mathbf{a}) = \mathcal{F}\{f(\mathbf{x})\}$ and $\tilde{g}(\mathbf{a}) = \mathcal{F}\{g(\mathbf{x})\}$. If the two spectra are strongly correlated with one another, one would observe a bright correlation peak in the output plane. This is the idea behind the VanderLugt optical correlator [2]. However, at the origin where $\mathbf{a} = 0$ the expression in Eq. (3) reduces to an inner product integral. In other words, one can implement an inner product, provided that one only measures the light at the center of the back focal (Fourier) plane.

This method has been used to implement inner products in classical systems to measure the modal content of optical beam profiles [3,9]. In such cases the output in the back focal plane (Fourier plane) is measured by a charge-coupled-device (CCD) camera and the intensity that is measured by the pixel at the origin represents the squared modulus of the result of the inner product. The area of the pixel must be comparable to one resolution cell in the output plane of the system. A resolution cell is the area covered by the Fourier transform of the limiting aperture (exit pupil) of the optical system.

### B. Imaging onto SMF

Another method used to implement the integration process is to image the light onto the end of the SMF, as shown in Fig. 2. The SMF guides the photons that are coupled into the fiber onto an avalanche photodiode. This method is often employed in quantum optical applications where, instead of the CCD camera, a detection system is needed that can detect single photons with adequate efficiency.

The overlap integral that gives the coupling coefficient (which is also an inner product) is

$$\eta = \iint p(\mathbf{u})G(\mathbf{u};w)\,d^2x, \tag{4}$$

where $\eta$ is the coupling efficiency, $p(\mathbf{u})$ is a normalized version [as in Eq. (2)] of the complex-valued optical field that illuminates the end of the SMF, $\mathbf{u}$ represents the transverse coordinates on the end of the SMF, and

$$G(\mathbf{u};w) = \frac{1}{w}\sqrt{\frac{2}{\pi}}\exp\left(-\frac{|\mathbf{u}|^2}{w^2}\right) \tag{5}$$

is the normalized mode of the SMF, with $w$ being the size of the mode on the end of the SMF.

In the optical system the imaging is usually done with the aid of a 4-f system, as shown in Fig. 2, which relays the image of the product of the two functions $f(\mathbf{x})g^*(\mathbf{x})$ onto the end of the SMF, using an appropriate demagnification. Evaluating the resulting overlap integral on the plane of the SLM,[2] we obtain

$$\eta = \mathcal{N}\iint f(\mathbf{x})g^*(\mathbf{x})G(\mathbf{x};W)\,d^2x, \tag{6}$$

[2]The same result for the coupling coefficient is obtained regardless of the plane on which it is evaluated, provided that all the functions are correctly transformed to that plane.

where $W$ is the size of the mode when imaged (magnified) backward onto the SLM and $\mathcal{N}$ is a normalization constant for the product of $f(\mathbf{x})$ and $g^*(\mathbf{x})$

$$\mathcal{N} = \left[\iint |f(\mathbf{x})g^*(\mathbf{x})|^2 \, d^2x\right]^{-1/2}. \tag{7}$$

Note that although $f(\mathbf{x})$ and $g(\mathbf{x})$ may be individually normalized, their product in general is not. The optical power that is coupled into the SMF and measured by the detector is given by $P_{\text{SMF}} = |\eta|^2 P_{\text{in}}$ where $P_{\text{in}}$ is the total incident power falling on the end of the SMF.

Since the expression in Eq. (6) plays an important role in the following discussions, we provide a specific notation for it. The Gaussian distorted inner product (GDIP) is defined as

$$\langle f,g;W\rangle_G \equiv \iint f(\mathbf{x})g^*(\mathbf{x})G(\mathbf{x};W)\, d^2x. \tag{8}$$

It then follows that one can express Eq. (6) as

$$\eta = \mathcal{N}\langle f,g;W\rangle_G. \tag{9}$$

While the inner product in Eq. (1) allows one to separate the contributions of orthogonal basis functions, the coupling coefficient, as given by Eq. (6), is indifferent to whether $f(\mathbf{x})$ and $g(\mathbf{x})$ are orthogonal or not. Only when the overlap integral becomes an inner product integral for $f(\mathbf{x})$ and $g(\mathbf{x})$, as in Eq. (1), can it extract the coefficients in a reliable way.

The expression in Eq. (6) would be an inner product integral if one can eliminate the Gaussian function $G(\mathbf{x};W)$ in some way. The simplest way to remove $G(\mathbf{x};W)$ is to absorb it into $g^*(\mathbf{x})$. Hence, to compute the inner product between the beam profile $f(\mathbf{x})$ and a function $h(\mathbf{x})$, one would program the function $g^*(\mathbf{x}) \propto h^*(\mathbf{x})/G(\mathbf{x};W)$ onto the SLM, which follows from the identity

$$\langle f(\mathbf{x}),h(\mathbf{x})/G(\mathbf{x};W);W\rangle_G \equiv \langle f(\mathbf{x}),h(\mathbf{x})\rangle. \tag{10}$$

This approach is not always practical: due to the inverse of the Gaussian mode, $h^*(\mathbf{x})/G(\mathbf{x};W)$ tends to diverge for large $\mathbf{x}$. In the case where the spectrum is to be measured in terms of the Laguerre-Gaussian (LG) basis, one may be tempted to use the Gaussian mode from the SMF to represent the Gaussian envelope of the LG mode. Unfortunately, without the Gaussian envelope, the remaining part of the LG mode, which needs to be programed onto the SLM, is unbounded and diverges as one moves away from the origin.

An alternative approach is to expand the size of the Gaussian mode on the SLM by increasing the (de)magnification between the SLM and the SMF, so that the nonzero part of $fg^*$ is confined to the central part of the Gaussian mode where it is more or less constant. The resulting expression can then be approximated by

$$\eta \approx \frac{\mathcal{N}}{W}\sqrt{\frac{2}{\pi}}\iint f(\mathbf{x})g^*(\mathbf{x})\, d^2x, \tag{11}$$

which follows from the property

$$\langle f,g;W\rangle_G \overset{W\to\infty}{\longrightarrow} \frac{1}{W}\sqrt{\frac{2}{\pi}}\langle f,g\rangle. \tag{12}$$

The drawback is that the measured coupling efficiency is suppressed by a factor of $1/W$. In a practical experiment this implies low intensities or low photon counts, which would increase the sensitivity to noise.

Although the overlap integral in Eq. (4) is also an inner product, the coupling coefficient $\eta$ is in general not equal to the inner product $\langle f,g\rangle$. In some cases they are proportional to each other. For instance, when $G(\mathbf{x};W)$ is absorbed into $g^*(\mathbf{x})$, the inner product is given by $\langle f,h\rangle = \eta/\mathcal{N}$ and in the limit where $W$ is very large, the inner product is given by $\langle f,g\rangle = (\pi/2)^{1/2}W\eta/\mathcal{N}$.

### C. Fourier transform onto SMF

The optical system that is considered for the projective measurements in Ref. [6] is a combination of the above two systems: the Fourier transform of the product is coupling into a SMF. Such a system is modeled by

$$\eta = \mathcal{N}\iint\iint f(\mathbf{x})g^*(\mathbf{x})\exp[i2\pi(ax+by)] \times G\left(\mathbf{a};\frac{w}{f\lambda}\right) d^2x\, d^2a, \tag{13}$$

where $\mathbf{a} = \mathbf{u}/f\lambda$, with $f$ being the focal length of the Fourier transforming lens and $\lambda$ being the wavelength. Evaluating the integral over $\mathbf{a}$, one obtains

$$\eta = \mathcal{N}\iint f(\mathbf{x})g^*(\mathbf{x})G\left(\mathbf{x};w'\right)\, d^2x = \mathcal{N}\langle f(\mathbf{x}),g(\mathbf{x});w'\rangle_G, \tag{14}$$

where

$$w' = \frac{f\lambda}{\pi w}. \tag{15}$$

Equation (14) is equivalent to Eq. (6) with the substitution $W \to w'$. It also corresponds to Eq. (4) in Ref. [6], but in Eq. (14) the integral is evaluated on the SLM plane, instead of on the end of the SMF. As before, one can either absorb $G(\mathbf{x};w')$ into $g^*(\mathbf{x})$ or assume that $w'$ is large (which requires that one makes $f$ large), leading to the same drawbacks. In Ref. [6] the Gaussian mode is not absorbed into the function on the SLM and is allowed to have an arbitrary mode size.

Note that when $w'$ is large the resulting setup corresponds to the one modeled by Eq. (3) and shown in Fig. 1 but where the light is coupled into an SMF, instead of being registered by one CCD pixel. The implication is that while the single CCD pixel measures that total intensity of the light that falls on the surface of that one CCD pixel, the SMF only extracts the Gaussian component of the optical field that falls on its end.

### D. Modal transformation

There exists a more exact method to implement the required inner product when using SMFs. One can transform the mode that is to be detected into the Gaussian mode of the SMF. From a quantum mechanics perspective, such a process can be accomplished by a unitary transformation. In a physical optical system this process can be accomplished with the aid of two

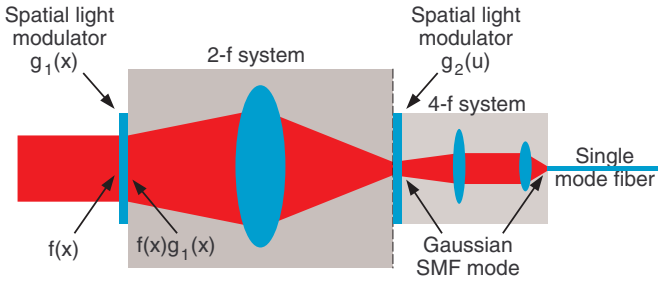


FIG. 3. (Color online) Diagram of a system that performs modal transformation to convert a particular mode $f(\mathbf{x}) = \Phi_n(\mathbf{x})$ into the SMF Gaussian mode. The two SLMs modulate their incident optical fields with $g_1(\mathbf{x}) = \exp[i\theta_1(\mathbf{x})]$ and $g_2(\mathbf{u}) = \exp[i\theta_2(\mathbf{u})]$, respectively.

SLMs, separated either by a distance of free-space propagation or by a 2-f system. The latter case is shown in Fig. 3. The purpose of the two SLMs is to introduce two phase functions that respectively transform the amplitude distribution and then the phase of the mode. The SMF Gaussian mode, which is obtained after the second SLM, is then imaged onto the end of the SMF by a 4-f system. Since, this process is unitary, any mode that is orthogonal to the mode that is being transformed into the Gaussian would be transformed into a mode that is orthogonal to the Gaussian and would therefore not be coupled into the SMF. In this way the system is able to extract the information associated with the particular mode without any cross-talk from other modes.

To determine the two required phase functions $\theta_1(\mathbf{x})$ and $\theta_2(\mathbf{u})$, one needs to solve the equation

$$G(\mathbf{u}; w) = \exp[i\theta_2(\mathbf{u})] \iint \Phi_n(\mathbf{x}) \exp[i\theta_1(\mathbf{x})] K(\mathbf{x},\mathbf{u})\, d^2x, \tag{16}$$

where $\Phi_n(\mathbf{x})$ is the mode to be converted into the Gaussian mode of the SMF and $K(\mathbf{x},\mathbf{u})$ is the kernel of the particular type of system (free-space propagation or 2-f Fourier transforming system). Equation (16) represents a potentially challenging inverse problem, akin to those associated with beam shaping [10], and needs to be solved for every mode to be detected with the inner product.

Due to the complexity associated with its implementation, this type of system is seldom used for the purpose of implementing inner products. However, see, e.g., [11].

### E. Entangled photon pairs

In many optical implementations of quantum information systems, entangled photon pairs are produced via spontaneous parametric down-conversion (PDC). Projective measurements are performed on the pair of entangled photons by making simultaneous measurements in the two down-converted beams of photons (the signal and idler beams). Each of the two measurements are done by modulating the beam with an SLM and coupling the result into an SMF. Usually the plane of the SLM is imaged by a 4-f system onto the end of the SMF. Most practical implementations of this experiment operate in the so-called thin crystal limit: the Rayleigh range of the pump beam is much larger than the thickness of the nonlinear crystal that mediates the PDC process. Within the thin crystal limit, the combined projective measurement for collinear PDC is expressed by a three-way overlap [12]

$$\alpha = \iint p(\mathbf{x}) m_s^*(\mathbf{x}) m_i^*(\mathbf{x})\, d^2x, \tag{17}$$

where $p(\mathbf{x})$ is the mode profile of the pump beam in the crystal plane, and $m_s(\mathbf{x})$ and $m_i(\mathbf{x})$ are the two modes on the crystal plane used for the projective measurement in the signal and idler beams, respectively. It is assumed that $p(\mathbf{x})$, $m_s(\mathbf{x})$, and $m_i(\mathbf{x})$ are normalized functions, as defined in Eq. (2). In practice, the latter two modes are introduced with the aid of the two SLMs and need to be transformed (imaged) onto the crystal plane for the calculation of the overlap with Eq. (17). Together with the Gaussian modes from the two SMFs, the actual integral becomes [13]

$$\alpha = \iint p(\mathbf{x}) m_s^*(\mathbf{x}) m_i^*(\mathbf{x}) G(\mathbf{x}; W)^2\, d^2x. \tag{18}$$

Here, $W$ is the mode size of the Gaussian modes when imaged back onto the crystal plane. As in Eq. (6), the correct overlap requires the removal of the Gaussian modes in Eq. (18). Usually the pump beam has a Gaussian profile. Therefore, one can absorb the two Gaussian modes from the two SMFs into the pump profile, which then modifies the latter's mode size, as follows:

$$\frac{1}{w_0^2} \to \frac{1}{w_0^2} + \frac{2}{W^2}, \tag{19}$$

where $w_0$ is the original pump beam radius. This method was used in Ref. [13] to obtain good agreement with experimental results. One can also absorb the Gaussian modes into the modes $m_s(\mathbf{x})$ and $m_i(\mathbf{x})$. However, in practice this is not always possible due to the tendency of the modified modal functions to diverge.

### F. Effect on orthogonality

In the two cases considered in Secs. II B and II C where an SMF is used to extract the Gaussian component, there are only two basic approaches to removing the Gaussian mode to obtain an inner product integral. Either the Gaussian is removed from the function on the SLM or the Gaussian is expanded so that it becomes a constant function over the support of the incident field. Depending on the application, neither of these approaches may be practical: the function on the SLM may diverge when one attempts to use it to remove the Gaussian, or the light levels may be too low when one expands the Gaussian, leading to unacceptably high noise sensitivity. For this reason, one may not have a choice but to accommodate the Gaussian modal overlap inside the inner product integral, given by the expression in Eq. (6). It is precisely this scenario that is considered in Ref. [6]. However, the situation is more complicated than a mere drop in the coupling coefficient. If the reduction in the coupling coefficient were the only problem, one could remove it as follows:

$$\eta = \frac{\mathcal{N}_f \langle f, \Phi_n; W\rangle_G}{\mathcal{N}_n \langle \Phi_n, \Phi_n; W\rangle_G}, \tag{20}$$

where $\Phi_n$ is a basis function and $\mathcal{N}_f$ and $\mathcal{N}_n$ are the normalization constants associated with the numerator and denominator, respectively.

The problem is not only the reduction in the coupling efficiency, but also the cross-talk that is introduced between different basis functions due to the Gaussian distortion in the inner product. Basis functions that were supposed to be orthogonal are not in general orthogonal anymore. For the case of an OAM basis such as the LG modes considered in Ref. [6], the orthogonality between modes with different azimuthal indices remains in tact, but the orthogonality between modes with the same azimuthal indices and different radial indices is lost.

Hence, if the input field only consists of LG modes with the same radial index, then the inclusion of the Gaussian overlap in the inner product will not adversely affect the extraction process, provided that one uses Eq. (20) to correct the value of the coefficients. Unfortunately, it is unlikely in a practical experiment that one can ever assume that the incident field only consists of LG modes with the same radial index. When the input field $f(\mathbf{x})$ contains LG modes with arbitrary radial indices, the coefficient that is extracted by the GDIP for a particular azimuthal index $\langle f(\mathbf{x}), M_p; W\rangle_G$ will consist of an unknown linear combination of coefficients, associated with the same azimuthal index but different radial indices

$$\langle f(\mathbf{x}), M_p; W\rangle_G = \sum_q \alpha_q \langle M_q, M_p; W\rangle_G, \tag{21}$$

where $\alpha_q$ denotes the coefficients. The two LG modes $M_p = M_{\mathrm{LG}}(\mathbf{x}; p,\ell)$ and $M_q = M_{\mathrm{LG}}(\mathbf{x}; q,\ell)$ have the same azimuthal index $\ell$ and different radial indices $p$ and $q$. The nonzero overlap from the GDIP between LG modes with the same azimuthal index and different radial indices is indicated by $\langle M_q, M_p; W\rangle_G = \mathcal{M}_{pq}$. To unravel the coefficients for the different radial indices in such a case, one needs to invert the matrix $\mathcal{M}_{pq}$. Hence, the benefit of using an orthogonal basis is lost.

One can still obtain a reliable description of the density matrix from quantum state tomography under these circumstances, but one needs to take the effect of the nonorthogonality into account to obtain an accurate description of the measurement process in terms of positive-operator valued measures [14].

## III. ANALYSIS

### A. Analytical expressions

To investigate how serious this situation is, we analyze the expression of the GDIP in Eq. (8) for the LG basis for arbitrary azimuthal and radial indices. We do this with the aid of a generating function for the LG modes at $z = 0$, which is given by [13,15]

$$\mathcal{G} = \frac{1}{1-\eta}\exp\left[\frac{(x \pm iy)\mu}{(1-\eta)w_0} - \frac{(x^2+y^2)(1+\eta)}{(1-\eta)w_0^2}\right], \tag{22}$$

where $\mu$ and $\eta$ are generating parameters for the azimuthal and radial indices, respectively, the sign in the exponent is given by the sign of azimuthal index $\ell$, and $w_0$ is the radius of the beam waist. For particular values of the mode indices $p$ and $\ell$, the LG mode is obtained by

$$M_{\mathrm{LG}}(\mathbf{x}; p,\ell) = \frac{\mathcal{N}_{\mathrm{LG}}}{p!}\left[\frac{\partial^p}{\partial\eta^p}\frac{\partial^{|\ell|}}{\partial\mu^{|\ell|}}\mathcal{G}\right]_{\eta,\mu=0}, \tag{23}$$

where

$$\mathcal{N}_{\mathrm{LG}} = \left[\frac{2\pi 2^{|\ell|}p!}{(p+|\ell|)!}\right]^{1/2} \tag{24}$$

is the modal normalization constant.

The result, after evaluating the integral in Eq. (8) with the aid of Eqs. (5) and (22), is expressed as a generating function of the GDIP for different radial indices

$$\mathcal{G}_{\mathrm{G}} = \frac{2^{1+|\ell|}(|\ell|)!\sqrt{\alpha}}{[2(1-\eta_1\eta_2)+\alpha(1-\eta_1)(1-\eta_2)]^{1+|\ell|}}, \tag{25}$$

where[3] $\alpha = w_0^2/W^2$ and $\eta_1$ and $\eta_2$ are the generating parameters for the input and output radial indices, respectively. The result for a particular set of radial indices $p$ and $q$ are obtained from the following calculation:

$$\langle M_p, M_q; W\rangle_G = \mathcal{N}_{pq}\left[\frac{\partial^p}{\partial\eta_1^p}\frac{\partial^q}{\partial\eta_2^q}\mathcal{G}_{\mathrm{G}}\right]_{\eta_{1,2}=0}. \tag{26}$$

The normalization constant $\mathcal{N}_{pq}$ is obtained from Eq. (7), where we again use generating functions to represent the four LG modes with the same azimuthal index, but arbitrary radial indices. The resulting generating function for the normalization constant is

$$\mathcal{G}_{\mathcal{N}} = \frac{(2|\ell|)!(\nu_1\nu_2\nu_3\nu_4)^{1+|\ell|}}{(\nu_1+\nu_2+\nu_3+\nu_4-2)^{1+2|\ell|}}, \tag{27}$$

where $\nu_n = 1/(1-\eta_n)$. The normalization constant is produced by

$$\mathcal{N}_{pq} = \left[\frac{\partial^p}{\partial\eta_1^p}\frac{\partial^q}{\partial\eta_2^q}\frac{\partial^p}{\partial\eta_3^p}\frac{\partial^q}{\partial\eta_4^q}\mathcal{G}_{\mathcal{N}}\right]^{-1/2}_{\eta_{1,2,3,4}=0}. \tag{28}$$

### B. Results

In Fig. 4 we show three different cases where we plot the modulus squared GDIP between two LG modes with the same azimuthal index. In each graph the one LG mode has a fixed radial index $p$, while the radial index of the other mode $q$ varies from 0 to 5. All graphs are shown as a function of the squared mode size ratio $\alpha = w_0^2/W^2$. Since these values are all computed with normalized functions, the maximum value that can be obtained is 1.

In Fig. 4(a) we show the case for $\ell = 0$ and $p = 0$. One can see that the largest overlap appears when $p = q = 0$. However, the cases where $p \neq q$ are not zero as one would have found for an accurate inner product. In other words, the LG modes with different radial indices are not orthogonal with respect to the GDIP. The $(p = q = 0)$ curve reaches a value of 1 at $\alpha = 2$. This implies that for $\ell = 0$ and $p = 0$ the point where $\alpha = 2$ $(w_0 = \sqrt{2}W)$ produces a product $fg^*$ that exactly matches

[3] In the notation of [6]: $\alpha = 2\sigma^2/a_0^2$.

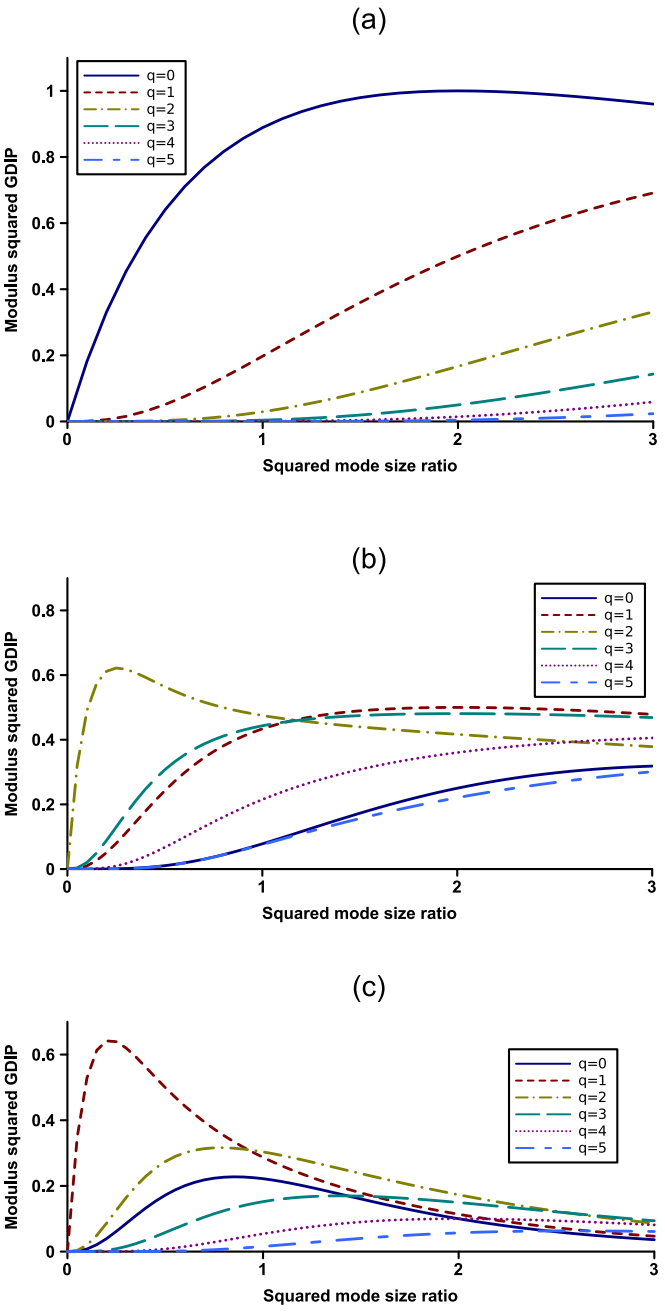


FIG. 4. (Color online) GDIP as a function of the squared mode size ratio $\alpha$, showing the overlap between two LG modes. In all three graphs, the two LG modes have the same azimuthal index: (a) $\ell = 0$, (b) $\ell = 1$, and (c) $\ell = 3$. The radial index for one LG mode is (a) $p = 0$, (b) $p = 2$, and (c) $p = 1$. The radial index of the other LG mode ranges over $q = 0$–5 in all three graphs.

the SMF Gaussian mode. This is a unique case that is not reproduced for any other LG mode.

In Fig. 4(b) we considered the case where $\ell = 1$ and $p = 2$. In this case the largest overlap occurs for $p = q = 2$, as expected. Again the cases where $p \neq q$ are not zero. They are in fact quite large and become larger than the $(p = q)$ case for $\alpha \gtrsim 1$. The maximum value of the GDIP that is obtained for the LG mode with $\ell = 1$ and $p = 2$ is much smaller than 1. The reason is that the product $fg^*$ does not exactly match the SMF Gaussian mode.

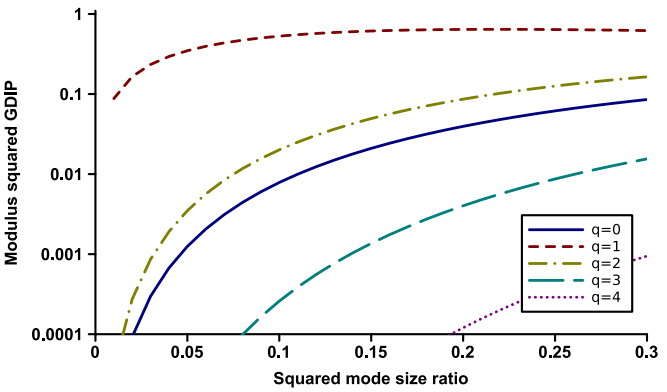


FIG. 5. (Color online) Curves for $q = 0.4$, as in Fig. 4(c), but with a logarithmic vertical scale and for small values of $\alpha$.

The case where $\ell = 3$ and $p = 1$ is shown in Fig. 4(c). Again, as expected, the largest overlap occurs for $p = q = 1$ and the cases where $p \neq q$ are not zero. Instead, the latter curves become larger than the $(p = q)$ case for $\alpha \gtrsim 1$. As in Fig. 4(b), the maximum value that is obtained for the LG mode with $\ell = 3$ and $p = 1$ is significantly smaller than 1, because the product $fg^*$ does not match the SMF Gaussian mode.

In all the cases shown in Fig. 4, one can see that the curves for $p \neq q$ are suppressed as $\alpha \to 0$. This confirms the statement that an accurate inner product can be implemented by having a small enough value for $\alpha$. In other words, when the SMF mode is small compared to the size of the Fourier transform of the product $fg^*$, one can implement an accurate inner product, as discussed in Secs. II A and II C. To demonstrate this tendency, we show in Fig. 5 the suppression of the $(p \neq q)$ curves, compared to the $(p = q)$ curve, by plotting the curves of Fig. 4(c) with a logarithmic vertical scale over a range of small values for $\alpha$. Note how much the $(p \neq q)$ curves are suppressed compared to the $(p = q)$ curve, as $\alpha \to 0$.

## IV. SUMMARY AND CONCLUSIONS

The practical optical implementation of inner products for the purpose of projective measurements in classical or quantum optical systems is discussed. We explain a number of different methods to implement accurate inner products. However, these implementations are often not practical. For this reason we analyze, for the LG basis, the consequences of the inaccuracy caused by the overlap with the Gaussian mode of an optical fiber, which results in the so-called Gaussian distortion of the inner product. We show that this distorted version of the inner product not only causes a reduced coefficient for the overlap, as reported before [6], but also a loss of orthogonality between modes with different radial indices of the LG modes. These effects are analyzed quantitatively to demonstrate their severity. We also point out that one can reduce these effects with an optimal choice for the mode sizes.

Although we only considered the LG basis here, the same arguments can be made for other bases, such as the Bessel-Gaussian basis [8], which is another OAM basis. In such a case the radial degree of freedom is governed by a continuous parameter instead of a discrete index.

[1] D. F. V. James, P. G. Kwiat, W. J. Munro, and A. G. White, Phys. Rev. A **64**, 052312 (2001); B. Jack, J. Leach, H. Ritsch, S. M. Barnett, M. J. Padgett, and S. Franke-Arnold, New J. Phys. **11**, 103024 (2009); M. Agnew, J. Leach, M. McLaren, F. S. Roux, and R. W. Boyd, Phys. Rev. A **84**, 062101 (2011).

[2] A. Vander Lugt, IEEE Trans. Info. Theory **10**, 139 (1964); J. L. Horner and P. D. Gianino, Appl. Opt. **23**, 812 (1984).

[3] F. S. Roux, Appl. Opt. **35**, 1894 (1996); **35**, 4610 (1996).

[4] T. Kaiser, D. Flamm, S. Schröter, and M. Duparré, Opt. Express **17**, 9347 (2009).

[5] J. P. Torres, A. Alexandrescu, and L. Torner, Phys. Rev. A **68**, 050301 (2003); C. K. Law and J. H. Eberly, Phys. Rev. Lett. **92**, 127903 (2004); F. M. Miatto, A. M. Yao, and S. M. Barnett, Phys. Rev. A **83**, 033816 (2011).

[6] H. Qassim, F. M. Miatto, J. P. Torres, M. J. Padgett, E. Karimi, and R. W. Boyd, J. Opt. Soc. Am. B **31**, A20 (2014).

[7] L. Allen, M. W. Beijersbergen, R. J. C. Spreeuw, and J. P. Woerdman, Phys. Rev. A **45**, 8185 (1992).

[8] F. Gori, G. Guattari, and C. Padovani, Opt. Commun. **64**, 491 (1987).

[9] D. Flamm, D. Naidoo, C. Schulze, A. Forbes, and M. Duparré, Opt. Lett. **37**, 2478 (2012); I. A. Litvin, A. Dudley, F. S. Roux, and A. Forbes, Opt. Express **20**, 10996 (2012).

[10] F. M. Dickey and S. C. Holswade, *Laser Beam Shaping: Theory and Techniques* (CRC, Boca Raton, FL, 2002).

[11] G. Molina-Terriza, A. Vaziri, J. Řeháček, Z. Hradil, and A. Zeilinger, Phys. Rev. Lett. **92**, 167903 (2004).

[12] M. McLaren, J. Romero, M. J. Padgett, F. S. Roux, and A. Forbes, Phys. Rev. A **88**, 033818 (2013).

[13] Y. Zhang, F. S. Roux, M. McLaren, and A. Forbes, Phys. Rev. A **89**, 043820 (2014).

[14] M. A. Nielsen and I. L. Chuang, *Quantum Computation and Quantum Information* (Cambridge University, Cambridge, England, 2000).

[15] F. S. Roux, Phys. Rev. A **83**, 053822 (2011); Y. Zhang and F. S. Roux, *ibid.* **89**, 063802 (2014).